PHYSICAL REVIEW C VOLUME 44, NUMBER 6 DECEMBER 1991

Coulomb distortion effects in $(e,e'\gamma)$ processes

Indu Talwar
Computer Science Department, State University of New York at Geneseo, New York 14454

Amirul Hoque and L. E. Wright
Physics Department, Ohio University, Athens, Ohio 45701
(Received 17 June 1991)

Using Coulomb distorted waves for the electron wave functions, we investigate $(e,e'\gamma)$ processes where the nucleus is excited by inelastic electron scattering and the subsequent decay photon is detected in coincidence with the scattered electron with the nonavoidable bremsstrahlung process which must be coherently included. We examine the effects of Coulomb distortion on the resulting cross sections and compare our results with plane-wave analyses and with previous approximate calculations. In addition to examining other calculations, we compare our results with the available data and discuss the possibilities of using this reaction to determine multipole admixtures and extracting transition charge and current distributions for medium and heavy nuclei.

I. INTRODUCTION

For many years electron scattering has been one of the most important tools for investigating nuclear structure. The principle reasons for this are that the electromagnetic interaction is well understood and that it is relatively weak, so that it only slightly disturbs the nucleus under study and penetrates the entire volume. While phase-shift analysis is necessary for the analysis of elastic electron scattering, the plane-wave Born approximation (PWBA) suffices for the analysis of inelastic electron scattering from light nuclei. For inelastic electron scattering from medium and heavy nuclei, it was necessary to include Coulomb distortion in the electron wave functions and carry out a distorted-wave Born approximation (DWBA) analysis. This was worked out many years ago [1], and more recently, a Coulomb distorted analysis of the radiation tail accompanying elastic scattering [2] which lies under the inelastic cross section justified an *ad hoc* procedure long used for subtracting the radiation tail from medium and heavy nuclei [3]. Using these tools, inelastic electron scattering has become a very precise tool for extracting the radial distributions of transition charge and current distributions to nuclear levels, particularly for cases when only one multipole transition is allowed or dominant.

With the advent of new continuous-beam machines, coincidence experiments of the form $(e,e'x)$ become possible. In most cases particle x is some nucleon knocked out of the nucleus or a meson produced from a bound nucleon, which then exits the system. In both cases the coincidence requirement eliminates the troublesome radiation tail, but having a hadron as an outgoing particle introduces the traditional uncertainties arising from the strong interaction. While many interesting experiments are being done with x being a hadron, the idea of keeping the precision and the lack of uncertainty associated with purely electromagnetic interactions is difficult to give up.

The basic features of $(e,e'\gamma)$ were first explored by Rose and co-workers [4,5] in the plane-wave electron approximation. They identified the essential properties of the process and treated both the problem of bremsstrahlung-nuclear interference and the case of nonzero spin nuclei. Subsequently, Drechsel and Überall [6] extended the plane-wave analysis to overlapping nuclear levels, while Arenhövel and Drechsel [7] formulated the problem in the language of polarizabilities. More recently, Fein *et al.* [8] have used this approach to examine the suitability of $(e,e'\gamma)$ as a probe for giant resonances. Finally, within the plane-wave approach, Donnelly, Raskin, and Dubach [9] have emphasized the complementarity between the $(e,e'\gamma)$ process and electron scattering from polarized targets. An early work [10] set up the basic formalism for including Coulomb distortion in the nuclear part of the process, but investigated only a few cases. More recently, Ravenhall *et al.* [11], in collaboration with the experimentalists at the University of Illinois, have included the Coulomb distortion effects on the part of the transition induced by the charge operator in the Coulomb gauge. They avoided kinematic regions where the bremsstrahlung interference is a significant contribution. To date, the experimental efforts to use the $(e,e'\gamma)$ reaction have been carried out at Illinois [12] and Mainz [13]. While both groups reported that accurate measurements of the process are difficult, they were able to obtain quite good data from an $E2$ transition in ^{12}C and a mixed $E2$-$M1$ transition in ^{15}N. The primary experimental difficulty, apart from rather low counting rates, is the detection of the coincidence gamma rays in the hostile environment of an electron-scattering hall. However, as noted by Papanicolas in an invited talk four years ago [14], with care the reaction $(e,e'\gamma)$ can be effectively used to study nuclear excitations below the particle-emission threshold to a high degree of accuracy even for mixed-multipole transitions.

With the intention of helping achieve this possibility,

we will examine the $(e,e'\gamma)$ reaction with the inclusion of the bremsstrahlung amplitude in both the plane-wave approximation and with Dirac Coulomb waves for the electron. Inclusion of the bremsstrahlung amplitude will increase the kinematic region available to the experimentalists since useful coincidence data can be obtained nearer the incident and scattered electron directions, and inclusion of Coulomb distortion in both the nuclear excitation and bremsstrahlung amplitudes will permit the analysis of experiments from medium and heavy nuclei. In the present work, we restrict ourselves to particle stable states where the resolution of the detectors is greater than the natural decay width of the states. This permits us to only calculate the amplitude corresponding to nuclear excitation followed by subsequent decay since the time-reversal amplitude is very small. Our purpose is to fit the available data and to examine a number of nuclear transitions, particularly mixed-multipole transitions, to see if $(e,e'\gamma)$ can be useful in extracting the nuclear transition and current distributions. We also have particular interest in the case of heavy nuclei since the bremsstrahlung amplitude is proportional to Z, while the nuclear excitation and decay is proportional, roughly speaking, to the number of nucleons involved in the transition. Thus the bremsstrahlung amplitude increases relative to a single-particle transition and subsequent decay. Furthermore, both are modified by Coulomb distortion. One of our goals is to see how useful $(e,e'\gamma)$ is for such cases.

In Sec. II we give our formalism for describing the $(e,e'\gamma)$ process in both the plane-wave approximation and DWBA. We include both the nuclear excitation and subsequent decay amplitude and the bremsstrahlung amplitude. In Sec. III we present a number of examples to illustrate the application of the $(e,e'\gamma)$ process to the study of real nuclei, including mixed-multipole transitions. In Sec. IV we briefly summarize our conclusions.

II. FORMALISM

A. Nuclear excitation amplitude

The Hamiltonian density representing the interaction of electron and nucleus due to exchange of one photon of momentum k is

$$H_{\rm int}^{(n)} = -4\pi\alpha[\rho_e^{\rm op} G(\mathbf{r}_e,\mathbf{r}_n)\rho_n^{\rm op}(\mathbf{r}_n) - \mathbf{j}_e^{\rm op}\cdot\mathbf{G}(\mathbf{r}_e,\mathbf{r}_n)\cdot\mathbf{j}_n^{\rm op}(\mathbf{r}_n)] , \quad (1)$$

where $\rho_e^{\rm op}$ and $\mathbf{j}_n^{\rm op}$ ($\rho_n^{\rm op}$ and $\mathbf{j}_n^{\rm op}$) are electron (nuclear) charge and current-density operators and α is the fine-structure constant. The Green's functions G and $\mathbf{G}$ for the interaction are given by

$$G(\mathbf{r}_e,\mathbf{r}_n) = ik\sum_{LM} j_L(kr_<)h_L^{(1)}(kr_>)Y_L^M(\hat{r}_e)Y_L^{*M}(\hat{r}_n) , \quad (2)$$

for the charge-charge interaction, and

$$\mathbf{G}(\mathbf{r}_e,\mathbf{r}_n) = ik\sum_{JLM} j_L(kr_<)h_L^{(1)}(kr_>)\mathbf{Y}_{JL}^M(\hat{r}_e)\mathbf{Y}_{JL}^{*M}(\hat{r}_n) , \quad (3)$$

for the current-current interaction, where $r_<$ and $r_>$ refer to the larger or smaller of $\mathbf{r}_e$ and $\mathbf{r}_n$. They are given by an expansion into spherical harmonics, which also separates the nuclear and the electron variables. Using Ψ and ψ to denote the time-independent nuclear and electron wave functions, the amplitude for transitions from the initial state i into the final state f' is

$$A_{if'}^{(n)} = -4\pi\alpha\int\int[\langle\psi_{f'}|\rho_e^{\rm op}|\psi_i\rangle G(\mathbf{r}_e,\mathbf{r}_n)\langle\Psi_{f'}|\rho_n^{\rm op}|\Psi_i\rangle - \langle\psi_{f'}|\mathbf{j}_e^{\rm op}|\psi_i\rangle\cdot\mathbf{G}(\mathbf{r}_e,\mathbf{r}_n)\cdot\langle\Psi_{f'}|\mathbf{j}_n^{\rm op}|\Psi_i\rangle]d\tau_n,d\tau_e . \quad (4)$$

The matrix elements $\langle\psi_{f'}|\rho^{\rm op}|\psi_i\rangle$ and $\langle\psi_{f'}|\mathbf{j}^{\rm op}|\psi_i\rangle$ are the transition charge and current densities, respectively. For the electron these quantities are simply evaluated:

$$\langle\psi_{f'}|\rho_e^{\rm op}|\psi_i\rangle = \psi_{f'}^\dagger(\mathbf{r}_e)\psi_i(\mathbf{r}_e) , \quad (5)$$

$$\langle\psi_{f'}|\mathbf{j}_e^{\rm op}|\psi_i\rangle = \psi_{f'}^\dagger(\mathbf{r}_e)\boldsymbol{\alpha}\psi_i(\mathbf{r}_e) , \quad (6)$$

where $\boldsymbol{\alpha}$ is the Dirac matrices. For the nucleus, transition densities are conveniently expressed by employing the expansions

$$\langle\Psi_{f'}|\rho_n^{\rm op}|\Psi_i\rangle = \sum_{L,M} C_{M_iMM_{f'}}^{J_iLJ_{f'}}\rho_L(r_n)Y_L^M(\hat{r}_n) , \quad (7)$$

$$\langle\Psi_{f'}|\mathbf{j}_n^{\rm op}|\Psi_i\rangle = \sum_{L,M} C_{M_iMM_{f'}}^{J_iLJ_{f'}}[J_{L,L}(r_n)\mathbf{Y}_{L,L}^M(\hat{r}_n) + J_{L,L-1}(r_n)\mathbf{Y}_{L,L-1}^M(\hat{r}_n) + J_{L,L+1}(r_n)\mathbf{Y}_{L,L+1}^M(\hat{r}_n)] . \quad (8)$$

The strength of the transitions are characterized by the reduced transition probabilities for electric and magnetic multipoles defined by

$$B(EL;J_i\to J_f) = \frac{2J_i+1}{2J_f+1}\left[\frac{(2L+1)!!}{\omega^L}\int_0^\infty r^2dr\,\rho_L(r)j_L(\omega r)\right]^2 , \quad (9)$$

$$B(ML;J_i\to J_f) = \frac{2J_i+1}{2J_f+1}\left[\frac{L}{L+1}\right]\times\left[\frac{(2L+1)!!}{\omega^L}\int_0^\infty r^2dr\,J_{L,L}(r)j_L(\omega r)\right]^2 . \quad (10)$$

In Appendix A we define the form factor associated with these charge and current densities and give the constraints imposed by the continuity equation.

1. Plane-wave approximation

We give a brief review of the plane-wave Born approximation treatment of inelastic electron scattering, where we neglect the distortion of the electron wave functions by the static Coulomb field of the nucleus and take the electrons to be in plane-wave states. The wave function for an electron of momentum $\mathbf{p}$ and energy E may be written, for the initial state,

$$\psi_i^{(\uparrow\downarrow)}(\mathbf{p}_i,\mathbf{r}_e)=u_i^{(\uparrow\downarrow)}(\mathbf{p}_i)e^{i(\mathbf{p}_i\cdot\mathbf{r})} , \tag{11}$$

and for the final state

$$\psi_f^{(\uparrow\downarrow)}(\mathbf{p}_f,\mathbf{r}_e)=u_f^{(\uparrow\downarrow)}(\mathbf{p}_f)e^{i(\mathbf{p}_f\cdot\mathbf{r})} . \tag{12}$$

The spinors $u_{i(f)}^{(\uparrow\downarrow)}(\mathbf{p})$ are given for electrons traveling in general direction by

$$u_i^{(\uparrow)}=\left[\frac{E_i+m_e}{2m_e}\right]^{1/2}\begin{bmatrix}1\\0\\p_i\cos\theta_1/E_i+m_e\\p_i\sin\theta_1 e^{i\phi_1}/(E_i+m_e)\end{bmatrix} ,$$
$$u_i^{(\downarrow)}=\left[\frac{E_i+m_e}{2m_e}\right]^{1/2}\begin{bmatrix}0\\1\\p_i\sin\theta_1 e^{-i\phi_1}/E_i+m_e\\-p_i\cos\theta_1/(E_i+m_e)\end{bmatrix} , \tag{13}$$

$$u_f^{\dagger(\uparrow)}=\left[\frac{E_f+m_e}{2m_e}\right]^{1/2}\left[1\ 0\ \frac{p_f\cos\theta_2}{E_f+m_e}\ \frac{p_f\sin\theta_2 e^{-i\phi_2}}{E_f+m_e}\right] , \tag{14}$$

$$u_f^{\dagger(\downarrow)}=\left[\frac{E_f+m_e}{2m_e}\right]^{1/2}\left[0\ 1\ \frac{p_f\sin\theta_2 e^{i\phi_2}}{E_f+m_e}\ -\frac{p_f\cos\theta_2}{E_f+m_e}\right] . \tag{15}$$

The matrix elements for the scattering of the electrons by the nucleus can be written as

$$A_{if'}^{\rm ex}=-4\pi\alpha i\int\bar{u}_{p'}\int d\mathbf{r}\,e^{i\mathbf{q}\cdot\mathbf{r}}\left[\frac{\langle f'|\mathbf{j}_t|i\rangle\cdot\boldsymbol{\gamma}}{q^2-\omega^2}+\frac{i\langle f'|\rho_N|i\rangle}{q^2}\gamma_0\right]u_p , \tag{16}$$

where $\bar{u}=u^\dagger\gamma_0$ and $\boldsymbol{\alpha}=\beta\boldsymbol{\gamma}$. The multipole expansion of the Fourier transform of the nuclear matrix elements can be carried out by

$$\int_0^\infty\langle f'|\rho_N(\mathbf{r})|i\rangle e^{i\mathbf{q}\cdot\mathbf{r}}d\mathbf{r}=\sqrt{4\pi}\sum_{LM}\hat{L}i^L C_{M_jMM_{f'}}^{J_iLJ_{f'}}D_{M,0}^L(\theta,\phi,0)F_L^C(q) , \tag{17}$$

$$\int_0^\infty\langle f'|\mathbf{j}_t(\mathbf{r})|i\rangle e^{i\mathbf{q}\cdot\mathbf{r}}d\mathbf{r}=\sqrt{2\pi}\sum_{LM}\hat{L}i^L C_{M_iMM_{f'}}^{J_iLJ_{f'}}\sum_{\mu=\pm1}\mu D_{M,\mu}^L(\theta,\phi,0)\xi_\mu[F_L^M(q)+i\mu F_L^E(q)] , \tag{18}$$

where (θ,ϕ) are polar and azimuthal angle of $\mathbf{q}$ and the various form factors $F_L(q)$ are given in Appendix A. Choosing $\mathbf{q}$ along the z direction and substituting Eqs. (17) and (18) into Eq. (16), we obtain, for the excitation amplitude in the plane-wave approximation,

$$A_{if'}^{\rm ex}(M_i,M_{f'},m_i,m_{f'})=-4\pi\alpha i\sqrt{2\pi}\sum_{L,\mu}\bar{u}_{f'}\left[i^L C_{M_i\mu M_{f'}}^{J_iLJ_{f'}}\mu\hat{\boldsymbol{\xi}}\cdot\boldsymbol{\gamma}\frac{F_L^M(q)\hat{L}}{q^2-w^2}+iC_{M_i\mu M_{f'}}^{J_iLJ_{f'}}\mu\hat{\boldsymbol{\xi}}\cdot\boldsymbol{\gamma}\frac{F_L^E(q)}{q^2-w^2}+i\sqrt{2(2L+1)}C_{M_i0M_{f'}}^{J_iLJ_{f'}}\frac{F_L^c(q)}{q^2}\gamma_0\right]u_i , \tag{19}$$

where $\hat{\xi}_\mu$ are the spherical unit vectors given by $\hat{\xi}_1=-(\hat{x}+i\hat{y})/\sqrt{2}$, $\hat{\xi}_{-1}=(\hat{x}-i\hat{y})/\sqrt{2}$, $\hat{\xi}_0=\hat{z}$, and $\mu=\pm1$ in the transverse terms since $\mathbf{q}$ is along the z axis. The scattering amplitude can be separated into magnetic (transverse) and electric (transverse and longitudinal) components, which can be written as

$$A_M^{\rm ex}=-\frac{\sqrt{2L+1}}{q^2-\omega^2}i^L u_{f'}^\dagger(-C_{M_i1M_{f'}}^{J_iLJ_{f'}}\boldsymbol{\alpha}\cdot\hat{\boldsymbol{\xi}}_1+C_{M_i-1M_{f'}}^{J_iLJ_{f'}}\boldsymbol{\alpha}\cdot\hat{\boldsymbol{\xi}}_{-1})u_i F_L^M(q) , \tag{20}$$

$$A_E^{\rm ex}=-i^L\frac{F_L^E(q)}{q^2-\omega^2}u_{f'}^\dagger(C_{M_i1M_{f'}}^{J_iLJ_{f'}}\boldsymbol{\alpha}\cdot\hat{\boldsymbol{\xi}}_1+C_{M_i-1M_{f'}}^{J_iLJ_{f'}}\boldsymbol{\alpha}\cdot\hat{\boldsymbol{\xi}}_{-1})u_i+i^L\sqrt{2(2L+1)}\frac{F_L^c(q)}{q^2}C_{M_i0M_{f'}}^{J_iLJ_{f'}}u_{f'}^\dagger u_i . \tag{21}$$

2. Distorted wave

Next, we consider the distorted-wave treatment of inelastic electron scattering. That is, we take into account the distortion of an electron wave function due to the static Coulomb field of the nuclear charge density. The incoming and outgoing electron wave functions ψ_i and $\psi_{f'}$ are the solutions of the Dirac equation containing the potential due to static charge distribution of the nucleus. Explicitly, initial and final electron wave functions for electron momentum $p_i(p_{f'})$

and energy E_i ($E_{f'}$) in a central field when expanded in partial waves with appropriate boundary condition are

$$\psi_i^m(\mathbf{p}_i,\mathbf{r}_e)=4\pi\left[\frac{(E_i+m_e)}{2E_iV}\right]^{1/2}\sum_{\kappa\mu}e^{i\delta_\kappa}i^l C^{l(1/2)j}_{\mu-mm\mu}Y_l^{\mu-m*}(\hat{p}_i)\psi_\kappa^\mu(\mathbf{p}_i,\mathbf{r}_e)\ , \tag{22}$$

$$\psi_{f'}^{m'}(\mathbf{p}_f,\mathbf{r}_e)=4\pi\left[\frac{(E_f+m_e)}{2E_fV}\right]^{1/2}\sum_{\kappa'\mu'}e^{-i\delta_{\kappa'}}i^{l'}C^{l'(1/2)j'}_{\mu-m'm'\mu'}Y_{l'}^{\mu'-m'}(\hat{p}_f)\psi_{\kappa'}^{\mu'}(\mathbf{p}_{f'},\mathbf{r}_e)\ , \tag{23}$$

where the spinor is

$$\psi_\kappa^\mu(\mathbf{p}_i,\mathbf{r}_e)=\begin{bmatrix} g_\kappa(p_i,r_e)\chi_\kappa^\mu(\hat{r}_e) \\ if_\kappa(p_i,r_e)\chi_{-\kappa}^\mu(\hat{r}_e)\end{bmatrix}\ . \tag{24}$$

With these expansions the integration over the nuclear angular variables and the electron angular variables can be performed. In a coordinate system in which the incoming electron direction defines the z axis, one obtains the result

$$\begin{aligned}A^{\rm ex}_{J_iJ_{f'}}(M_i,M_{f'},m,m')=8\pi^2\alpha&\left[\frac{(E_i+m_e)(E_{f'}+m_e)}{(2J_i+1)E_iE_{f'}V^2}\right]^{1/2}\\ &\times\sum_{L,M}\frac{C^{J_iLJ_{f'}}_{M_iMM_{f'}}}{(2L+1)^{1/2}}\sum_{\kappa\kappa'}(-1)^{j'+l+1/2+l}e^{i(\delta_\kappa+\delta_{\kappa'})}i^{l-l'}(2l+1)(2j+1)^{1/2}\\ &\times C^{l(1/2)j}_{0mm}C^{l'(1/2)j'}_{m+M-m'm'm+M}C^{l'Lj'}_{mMm+M}\\ &\times[C^{lLl'}_{000}W(j'l'jl;\tfrac{1}{2}L)R^E(\kappa L\kappa')+C^{lL\bar{l}'}_{000}W(j'\bar{l}'jl;\tfrac{1}{2}L)R^M(\kappa L\kappa')]\\ &\times Y_{l'}^{m+M-m'}(\hat{p}_f)\ ,\end{aligned} \tag{25}$$

where $\bar{l}\equiv l(-\kappa)$ and the electric and magnetic radial integrals $R^E(\kappa L\kappa')$ and $R^M(\kappa L\kappa')$ are given by

$$\begin{aligned}R^E(\kappa L\kappa')=(2L+1)ik\int_0^\infty\int_0^\infty\Bigg[&\rho_L(r_n)j_L(kr_<)h_L^{(1)}(kr_>)[g_\kappa(r_e)g_{\kappa'}(r_e)+f_\kappa(r_e)f_{\kappa'}(r_e)]\\ &+i\frac{j_{L,L-1}(r_n)j_{L-1}(kr_<)h_{L-1}^{(1)}(kr_>)}{\sqrt{L(2L+1)}}\\ &\times\{L[f_\kappa(r_e)g_{\kappa'}(r_e)-g_\kappa(r_e)f_{\kappa'}(r_e)]+(\kappa-\kappa')[f_\kappa(r_e)g_{\kappa'}(r_e)+g_\kappa(r_e)f_{\kappa'}(r_e)]\}\\ &-i\frac{j_{L,L+1}(r_n)j_{L+1}(kr_<)h_{L+1}^{(1)}(kr_>)}{\sqrt{(L+1)(2L+1)}}\\ &\times\{(L+1)[f_\kappa(r_e)g_{\kappa'}(r_e)-g_\kappa(r_e)f_{\kappa'}(r_e)]-(\kappa-\kappa')[f_\kappa(r_e)g_{\kappa'}(r_e)+g_\kappa(r_e)f_{\kappa'}(r_e)]\}\Bigg]\\ &\times r_n^2r_e^2dr_ndr_e\end{aligned} \tag{26}$$

and

$$R^M(\kappa L\kappa')=(2L+1)ik\int_0^\infty\int_0^\infty i\frac{j_{L,L}(r_n)j_L(kr_<)h_L^{(1)}(kr_>)}{\sqrt{L(L+1)}}\{(\kappa+\kappa')[f_\kappa(r_e)g_{\kappa'}(r_e)+g_\kappa(r_e)f_{\kappa'}(r_e)]\}r_n^2r_e^2dr_ndr_e\ . \tag{27}$$

These particular forms of the radial integrals result from using the Lorentz gauge.

B. Deexcitation process

The nucleus γ decays from the excited state f' to state f with the emission of a photon and, of course, is independent of whether or not we use a plane wave or distorted wave for the excitation. The transition matrix element for the process is given by

$$A^{\rm dex}_{J_{f'}J_f}=-i\int d^4x\langle f,1|H_{\rm int}|0,f'\rangle e^{i(E_{f'}-E_f)t}\ , \tag{28}$$

where $H_{\rm int}=-\sqrt{4\pi\alpha}\,\mathbf{j}\cdot\mathbf{A}$, where $\mathbf{A}$ is the vector potential of the real photon field. In terms of the creation and annihilation operator, it can be written as

$$\mathbf{A}=\sum_{k,\lambda}(a_{k,\lambda}\vec{u}_{k,\lambda}e^{-i\omega t}+a^\dagger_{k,\lambda}\vec{u}^\dagger_{k,\lambda}e^{i\omega t})\ , \tag{29}$$

where $\vec{u}_{k,\lambda}=\hat{\epsilon}_\lambda e^{i\vec{k}\cdot\vec{r}}$ and λ denotes the polarization state of nuclear photons propagating with momentum $\mathbf{k}$:

$$A^{\rm dex}_{J_{f'}J_f}=-2\pi i\sqrt{4\pi\alpha}\,\delta(E_f+\omega-E_{f'})\int d^3r\langle f|\mathbf{j}\cdot\hat{\epsilon}^*_\lambda|f'\rangle e^{-i\mathbf{k}\cdot\mathbf{r}}\ . \tag{30}$$

We can expand the photon field $\hat{\epsilon}^* e^{-i\mathbf{k}\cdot\mathbf{r}}$ in terms of the multipole expansion

$$\hat{\epsilon}^* e^{-\mathbf{k}\cdot\mathbf{r}}=\lambda\sqrt{2\pi}\sum_{L,M}\hat{L}i^{-L}(-1)^{-M+1}D^{*L}_{-M,\lambda}(\phi_k,\theta_k,0)(\mathbf{A}^{\rm TM}_{LM}+i\lambda\mathbf{A}^{\rm TE}_{LM})\ , \tag{31}$$

where the radial parts of the current density are defined by the complex conjugate of Eq. (8) and the D function is defined by Rose [15]. The scattering amplitude thus is found to be

$$A^{\rm dex}_{J_{f'}J_f}(\lambda,M_{f'},M_f)=\frac{4\pi^2 i\lambda\sqrt{4\pi\alpha}}{\sqrt{(2J_{f'}+1)\omega}}\delta(E_f+\omega-E_{f'})$$
$$\times\sum_{LM}(-1)^{-M+1}i^{-L}D^{*L}_{-M,\lambda}(\phi_\gamma,\theta_\gamma,0)C^{J_{f'}LJ_f}_{M_{f'}MM_f}[\sqrt{2L+1}F^M_L(\omega)+i\lambda F^E_L(\omega)]\ . \tag{32}$$

In order to examine mixing between electric and magnetic multipoles, we separate this amplitude into magnetic and electric parts, both of which are transverse:

$$M^{\rm dex}_{J_{f'},J_f}(\lambda,M_{f'},M_f)=\frac{i\lambda(64\pi^5\alpha)^{1/2}}{\sqrt{(2J_{f'}+1)\omega}}\sum_{LM}i^{-L}e^{-iM\phi_\gamma}d^L_{\lambda-M}(\theta_\gamma)\hat{L}F^M_L(w)C^{J_{f'}LJ_f}_{M_{f'}MM_f} \tag{33}$$

and

$$E^{\rm dex}_{J_{f'},J_f}(\lambda,M_{f'},M_f)=\frac{i\lambda(64\pi^5\alpha)^{1/2}}{\sqrt{(2J_{f'}+1)\omega}}\sum_{LM}i^{-L}e^{-iM\phi_\gamma}d^L_{\lambda-M}(\theta_\gamma)F^E_L(\omega)C^{J_{f'}LJ_f}_{M_{f'}MM_f}\ . \tag{34}$$

For convenience, we introduce a mixing parameter β and write the total amplitude for excitation and deexcitation as

$$A^{\rm nucl}(\lambda,m,m',M_i,M_f,J_i,J_f)=\sum_{J_{f'}M_{f'}}[\beta E^{\rm ex}_{J_i,J_{f'}}(M_i,M_{f'},m,m')+(1-\beta)M^{\rm ex}_{J_i,J_{f'}}(M_i,M_{f'},m,m')]_q$$
$$\times[\beta E^{\rm dex}_{J_{f'},J_f}(\lambda,M_{f'},M_f)+(1-\beta)M^{\rm dex}_{J_{f'},J_f}(\lambda,M_{f'},M_f)]_\omega\ , \tag{35}$$

where the subscripts q and ω are the arguments of the form factors for the excitation (plane-wave case) and deexcitation amplitudes, respectively. The coincidence cross section is obtained by multiplying the excitation amplitude times the deexcitation amplitude and coherently summing over the angular momenta labels, L,L' and the intermediate magnetic substrates $M_{f'}$. Finally, the modulus squared of the product of the amplitudes is averaged over the initial spin states, summed over the final spin states, multiplied by the density of states, and divided by the incident flux to obtain

$$\frac{d^3\sigma_{\rm nucl}}{d\Omega_e d\Omega_\gamma d\omega}=\frac{\omega^2 p_f E_i E_f}{256 p_i\pi^7}\sum_{\substack{m_1m_2\\M_iM_f\lambda}}\left|\sum_{LL'M_{f'}}A^{\rm ex}_{L,M_i,M_{f'}}A^{\rm dex}_{L',M_{f'},M_f}\right|^2\ . \tag{36}$$

The deexcitation amplitude is the same for both the plane- and distorted-wave excitation, but one should note that, in the plane wave calculation, we choose the $\hat{\mathbf{z}}$ axis along $\mathbf{q}$ while in the distorted wave, we choose the $\hat{\mathbf{z}}$ axis along $\mathbf{p}_i$.

C. Bremsstrahlung amplitude

1. Distorted wave

The Hamiltonian density for electrons in a static electromagnetic field and photon is

$$H=H_{\rm rad}+H_{\rm DC}+H_{\rm int}\ , \tag{37}$$

where the spherical symmetric static Coulomb potential of the nucleus, $V(r)$, is included in the Dirac Coulomb Hamiltonian

$$H_{\rm DC}=-i\boldsymbol{\alpha}\cdot\boldsymbol{\nabla}+V(r)+m_e\beta\ , \tag{38}$$

and $\boldsymbol{\alpha}$ and β are the standard Dirac matrices. Substituting the partial-wave expansion Eqs. (22) and (23) for the initial and final electron states and the photon multipole expansion and carrying out the angular integral and requisite Dirac algebra, we obtain [2]

$$A_{fi}^{\text{bre}}(\lambda,M,L,m,m')=8\pi^3\lambda\left[\frac{(E_i+m_e)(E_f+m_e)\alpha}{E_fE_i\omega}\right]^{1/2}\times\sum_L\sqrt{2L+1}i^{-L}\sum_M(-1)^{-M+1}D^{*L}_{-M\lambda}(\phi_\gamma,\theta_\gamma,0)\times\sum_{\kappa,\kappa'}e^{i(\delta_\kappa+\delta_{\kappa'})}i^{l-l'}(-1)^{j+1/2}(2j+1)^{1/2}(2l+1)^{1/2}\times C^{l(1/2)j}_{0mM}C^{l'(1/2)j'}_{m+M-m'm'm+M}C^{jj'L}_{-(1/2)(1/2)0}C^{jLj'}_{mMm+M}\times R(\kappa,\kappa',L,\lambda)Y^{m+M-m'}_{l'}(\hat{p}_f)\ , \tag{39}$$

where the initial electron momentum $\mathbf{p}_i$ has been chosen to define the z axis. The radial integral in Eq. (39) is given by

$$R(\kappa,\kappa',L,\lambda)=\left[\frac{1+(-1)^{l+\bar{l}+L}}{2}\right]I^{(M)}+i\lambda\left[\frac{1+(-1)^{l+l'+L}}{2}\right]I^{(E)}\ , \tag{40}$$

where $\bar{l}=l(-\kappa)$, and the magnetic and electric radial integrals are given by

$$I^{(M)}=\frac{\kappa+\kappa'}{[L(L+1)]^{1/2}}\int_0^\infty j_L(\omega r)(f_\kappa g_{\kappa'}+g_\kappa f_{\kappa'}) \tag{41}$$

and

$$I^{(E)}=\left[\frac{L}{L+1}\right]^{1/2}\int_0^\infty\left[j_{L-1}(\omega r)\left[(f_\kappa g_{\kappa'}-g_\kappa f_{\kappa'})+\frac{\kappa+\kappa'}{L}(f_\kappa g_{\kappa'}+g_\kappa f_{\kappa'})\right]+j_L(\omega r)(f_\kappa g_{\kappa'}+g_\kappa f_{\kappa'})\right]r^2dr\ , \tag{42}$$

and for calculational convenience we have written the radial integrals in the least singular gauge.

The bremsstrahlung amplitude also can be expressed as a sum over the polar angle dependence of the D functions [15] by writing

$$a_{fi}=\sum_{L,M}a_{LM}d^L_{\lambda,-M}(\theta_\gamma)\ , \tag{43}$$

with the azimuthal dependence in the coefficient $a_{L,M}$. In this form we can apply the Yennie- Ravenhall [16] convergence technique to make the L sum converge faster. The recursion formula for $d^j_{m'm}(\theta)$ on j is given by

$$d^j_{m'm}(\theta_\gamma)\cos\theta_\gamma=\frac{a_1}{a_3}d^{j+1}_{m'm}(\theta_\gamma)\left[\frac{(j+m'+1)(j-m'+1)}{(j+m+1)(j-m-1)}\right]^{1/2}+\frac{a_4}{a_3}d^{j-1}_{m'm}\left[\frac{(j+m)(j-m)}{(j+m')(j-m')}\right]^{1/2}+\frac{a_2}{a_3}d^j_{m'm}(\theta_\gamma)\ , \tag{44}$$

where $a_1=[(j-m+1)(j+m+1)/(j+1)(2j+1)]a_3$, $a_4=[(j-m')(j+m')/j(2j+1)]a_3$, and $a_2=[mm'/j(2j+1)]a_3$. In our case, $j=L$, $m'=\lambda$, $m=-M$, and Eq. (44) reduces to

$$d^L_{\lambda,-M}(\theta_\gamma)\cos\theta_\gamma=\frac{\sqrt{(L+M+1)(L-M+1)(l+\lambda+1)(L-\lambda+1)}}{(L+1)(2L+1)}d^{L+1}_{\lambda,-M}(\theta_\gamma)+\frac{\sqrt{(L+M)(L-M)(L+\lambda)(L-\lambda)}}{(L+1)(2L+1)}d^{L-1}_{\lambda,-M}(\theta_\gamma)-\frac{M\lambda}{L(L+1)}d^L_{\lambda,-M}(\theta_\gamma)\ . \tag{45}$$

Equation (43) can be written as

$$a_{fi}=\frac{1}{(1-\cos\theta_\gamma)}\sum_{LM}a_{LM}(1-\cos\theta_\gamma)d^L_{\lambda,-M}(\theta_\gamma)\ , \tag{46}$$

and applying relation Eq. (45), we get

$$a_{fi}=\frac{1}{(1-\cos\theta_\gamma)}\sum_{L,M}a'_{L,M}d^L_{\lambda,-M}(\theta_\gamma)\ , \tag{47}$$

where

$$a'_{LM}=a_{LM}\left[1+\frac{M\lambda}{L(L+1)}\right]-a_{L-1M}\frac{\sqrt{(L+M)(L-M)(L+\lambda)(L-\lambda)}}{L(2L+1)}-a_{L+1M}\frac{\sqrt{(L+M+1)(L-M+1)(L+\lambda+1)(L-\lambda+1)}}{(L+1)(2L+1)}\ . \tag{48}$$

Using this technique, we can calculate the DWBA bremsstrahlung amplitude for all photon angles θ_γ at least 20°–30° from the incident and outgoing electron directions. For photon angles closer to either the incident or outgoing electron directions, the L series does not converge well.

2. *Plane-wave amplitude*

The transition matrix element for the second-order (bremsstrahlung) process is given by [2]

$$S_{fi}=i(4\pi\alpha)^{3/2}z\delta(E_f+\omega-E_i)\left[\frac{m^2}{2E_iE_f\omega}\right]^{1/2}\bar{u}_f(T_1+T_2)u_i\ . \tag{49}$$

The operators T_1 and T_2 corresponding to the two different diagrams appear between initial and final electron spinors with four-momenta $p_i=(E_i,\mathbf{p}_i)$ and $p_f+(E_f,\mathbf{p}_f)$ and can be written in terms of an integral over the intermediate three-momentum $\mathbf{p}$ as

$$T_1=\int\int d\mathbf{r}\,d\mathbf{p}\frac{\not\epsilon^*_\lambda(\gamma_0E_i-\boldsymbol{\gamma}\cdot\mathbf{p}+m)\gamma_0}{(\mathbf{p}_i^2-\mathbf{p}^2)|\mathbf{p}-\mathbf{p}_i|^2}F(|\mathbf{p}-\mathbf{p}_i|)e^{-i\mathbf{r}\cdot(\mathbf{k}-\mathbf{p}+\mathbf{p}_f)}\ , \tag{50}$$

$$T_2=\int\int d\mathbf{r}\,d\mathbf{p}\frac{\gamma_0(\gamma_0E_f-\boldsymbol{\gamma}\cdot\mathbf{p}+m)\not\epsilon^*_\lambda}{(\mathbf{p}_f^2-\mathbf{p}^2)|bp-\mathbf{p}_f|^2}F(|\mathbf{p}-\mathbf{p}_f|)e^{-i\mathbf{r}\cdot(\mathbf{k}+\mathbf{p}-\mathbf{p}_f)}\ , \tag{51}$$

where $F(q)=F(|\mathbf{p}-\mathbf{p}_i|)=F(|\mathbf{p}-\mathbf{p}_f|)$ is the form factor due to the finite size of the nucleus, λ denotes the photon polarization, and $\not\epsilon=\gamma_0\epsilon^0-\boldsymbol{\gamma}\cdot\hat{\xi}_\lambda$. After integrating over $\mathbf{r}$ and $\mathbf{p}$ and taking $\alpha^-=(\alpha_1-i\alpha_2)/\sqrt{2}$, $\boldsymbol{\gamma}=\beta\boldsymbol{\alpha}$, and $\gamma_0=\beta$, for positive λ, we obtain

$$S_{fi}^+=C(2\pi)^3\frac{F(q)}{q^2}u_f^\dagger\alpha^-\left[\frac{E_i+m\gamma_0+\alpha_1p_2\sin\theta_2e^{i\phi_2}+\alpha_3(p_2\cos\theta_2+\omega)}{p_i^2-(p_f^2+k^2+2p_fk\cos\theta_2)}\right.$$
$$\left.+\frac{E_f-m\gamma_0+\alpha_1p_1\sin\theta_1\cos\phi_1+\alpha_2p_1\sin\theta_1\sin\phi_1+\alpha_3(p_1\cos\theta_1-k)}{p_f^2-(p_i^2+k^2-2p_ik\cos\theta_\gamma)}\right]u_i\ , \tag{52}$$

and taking $\alpha^+=-(\alpha_1+i\alpha_2)/\sqrt{2}$, for negative λ, we obtain

$$S_{fi}^-=C(2\pi)^3\frac{F(q)}{\sqrt{2}q^2}u_f^\dagger\alpha^+\left[\frac{E_i+m\gamma_0+\alpha_1p_2\sin\theta_2e^{i\phi_2}+\alpha_3(p_2\cos\theta_2+k)}{p_i^2-(p_f^2+k^2+2p_fk\cos\theta_2)}\right.$$
$$\left.+\frac{E_f-m\gamma_0+\alpha_1p_1\sin\theta_\gamma\cos\phi_1+\alpha_3(p_1\cos\theta_1-k)+\alpha_2p_1\sin\theta_\gamma\sin\phi_1}{p_f^2-(p_i^2+k^2-2p_ik\cos\theta_\gamma)}\right]u_i\ , \tag{53}$$

where $C=i(4\pi\alpha)^{3/2}z\delta(E_f+\omega-E_i)$. The bremsstrahlung cross section can be written as an incoherent sum over the electron spins and photon polarization,

$$\frac{d^3\sigma_{\rm tot}}{d\Omega_e d\Omega_\gamma d\omega}=\sum_{m_1,m_2,\lambda}\left|A^\lambda_{m_1,m_2}\right|^2\ , \tag{54}$$

where

$$A^\lambda_{m_1,m_2}=\left[\frac{E_ik^2p_fE_f}{2p_i(2\pi)^7}\right]^{1/2}S^\lambda_{fi} \tag{55}$$

contains all flux, density of states, and statistical factors. Since the DWBA calculation for bremsstrahlung necessarily involves a photon multipole expansion, it is useful to obtain a multipole decomposition of the plane-wave result for checking purposes. We expand the photon field in multipoles by writing

$$\hat{\epsilon}^*_\mu e^{-i\mathbf{k}\cdot\mathbf{r}}=\mu\sqrt{2\pi}\sum_{L,M}\hat{L}i^{-L}(-1)^{-M+1}D^{*L}_{-M,\mu}(\hat{\mathbf{k}})$$
$$\times(\mathbf{A}^{\rm TM}_{LM}+i\mu\mathbf{A}^{\rm TE}_{LM})\ , \tag{56}$$

where $D^{*L}_{-M,\mu}(\hat{\mathbf{k}})$ are defined by Rose [16] and $\mathbf{A}^{\rm TM}_{LM}$ and $\mathbf{A}^{\rm TE}_{LM}$ are the transverse magnetic and electric Hansen solutions given by Eisenberg and Greiner [17]. The label μ denotes different polarization states of the photon. For $\mathbf{k}=\mathbf{p}_f-\mathbf{p}$ in T_1 and $\mathbf{k}=\mathbf{p}-\mathbf{p}_i$ in T_2, we can perform the space integrals in Eqs. (50) and (51). For example, the (TM) contribution to S^μ_{fi} for photon polarization is given by

$$(S^\mu_{fi})^{\rm TM}=C\sum_{L,M,\mu}\bar{u}_f[\not B^{LM}_{\lambda,\mu}(\not F_1+F_2^C)\gamma_0$$
$$+\gamma_0(\not F_2+F_2^C)\not B^{LM}_{\lambda,\mu}]u_i\ , \tag{57}$$

where

$$\mathcal{B}^{LM}_{\lambda,\mu}=[8\pi^5(2L+1)]^{1/2}(-1)^{L+M+1}D^{*L}_{-M,\mu}(\hat{\mathbf{k}})\hat{\xi}_\lambda \quad (58)$$

and $\hat{\xi}_\lambda$ are spherical basis vectors for $\lambda=0,\pm1$. The integrals over d^3p are written as a scaler integral $I_1^{LM\lambda}=C^{L1L}_{M-\lambda\lambda M}G_1^{LM\lambda}$, where

$$G_1^{LM-\lambda}=\int \frac{F(|\mathbf{p}-\mathbf{p}_i|)Y_L^{M-\lambda}(\hat{\mathbf{k}}_f)\delta(k-k_f)}{(\mathbf{p}_i^2-\mathbf{p}^2)|\mathbf{p}-\mathbf{p}_i|^2k^2}d^3p \ , \quad (59)$$

with $F_1^C=m_eI_1^{LM\lambda}$ and $F_1^0=E_iI_1^{LM\lambda}$ and vector integral $\mathbf{F}_1^{LM\lambda}=C^{L1\lambda}_{M-\lambda\lambda M}\mathbf{G}_1^{LM\lambda}$, where

$$\mathbf{G}_1^{LM-\lambda}=\int \frac{\mathbf{p}F(|\mathbf{p}-\mathbf{p}_i|)Y_L^{M-\lambda}(\hat{\mathbf{k}}_f)\delta(k-k_f)}{(\mathbf{p}_i^2-\mathbf{p}^2)|\mathbf{p}-\mathbf{p}_i|^2k^2}d^3p \ . \quad (60)$$

The integrals with the subscript 2 are obtained by interchanging the labels i and f for E_i, $\mathbf{p}_i$, and $\mathbf{k}_f$. The integrals $G_1^{LM-\lambda}$ and $\mathbf{G}_1^{LM-\lambda}$ can most easily be evaluated by choosing the vector $\mathbf{p}_i-\mathbf{p}_f$ to define the z axis and for $\mathbf{p}_i$ and $\mathbf{p}_f$ to lie in $x-z$ plane. It is convenient to take $\mathbf{k}_f$ as the integration variable rather than $\mathbf{p}$. The integration over dk_f is straightforwardly done by using the delta function [2]. The ϕ integration can be performed analytically by use of contour integration, while the remaining integration over θ is done numerically [2].

D. Interference and total cross section

For the case where the final nuclear state is the initial nuclear state, the amplitude for the nuclear excitation followed by deexcitation must be coherently added to the bremsstrahlung amplitude. Thus the cross section for this case is given by

$$\frac{d^3\sigma_{\rm tot}}{d\Omega_e d\Omega_\gamma d\omega}=\frac{\omega^2 p_f E_i E_f}{256 p_i \pi^7}\sum_{\substack{m,m',\lambda\\ M_i,M_f,J_i,J_f}}\left[\left|\sum_{L,M}A_{LM}^{\rm brem}\right|^2+\left|\sum_{L',M'}A_{L',M'}^{\rm nucl}\right|^2+\sum_{\substack{L,M\\ L'M'}}(A_{LM}^{*\rm brem}A_{L'M'}^{\rm nucl}+A_{LM}^{\rm brem}A_{L'M'}^{*\rm nucl})\right] . \quad (61)$$

However, when the final nuclear state is an excited nuclear state (not the ground state), there is no interference with bremsstrahlung. In the following we only consider the case where the nucleus returns to the ground state.

III. RESULTS AND DISCUSSION

Before examining specific cases, let us discuss the coordinate system for displaying results. We choose the incident electron to be along the z axis and the scattered electron lies in the x-z plane. Thus the momentum transfer $\mathbf{q}=\mathbf{p}_i-\mathbf{p}_f$ has azimuthal angle $\phi_q=\pi$. The outgoing photon is characterized by polar and azimuthal angles θ_γ and ϕ_γ, but for convenience in display, the in-plane photon distributions are plotted for θ_γ ranging from 0° to 360° with $\phi_\gamma=0$. Thus, in these plots, θ_q occurs somewhere between θ_γ equal to 180° and 360°. For photon distributions out of plane, we use the standard polar angles.

The formalism for the $(e,e'\gamma)$ process developed in the previous section is now used to explore the size of the corrections brought about by Coulomb distortion with the particular concern to see if the Coulomb effects interfere with using this reaction to study the underlying nuclear transitions. The ingredients needed for studying a given nuclear excitation and deexcitation process are multipole decomposed transition charge and current radial distributions. We used transition charge and current distributions extracted from inelastic scattering experiments, for the light nuclei ^{12}C and ^{15}N, a medium nucleus ^{90}Zr, and heavy nuclei ^{181}Ta and ^{208}Pb. In particular, we examine excitation and deexcitation of the 4.439-MeV, ($I^\pi=2^+$) state of ^{12}C, 6.32-MeV ($I^\pi=\frac{3}{2}^-$) state of ^{15}N, 5.06-MeV ($I^\pi=7^+$) state of ^{90}Zr, 0.136-MeV ($I^\pi=\frac{9}{2}^+$) state of ^{181}Ta, and 2.615-MeV ($I^\pi=3^-$) state of ^{208}Pb.

A. ^{12}C$(e,e'\gamma)(2^+,4.439\ \text{MeV})$

We first consider an $E2$ transition to the 4.439-MeV state in ^{12}C. We use the Fourier-Bessel fit to the transition charge and current distributions given by Ravenhall *et al.* [11] to characterize the transition. In Fig. 1(a) we show the coincidence differential cross sections for excitation and deexcitation, bremsstrahlung, and interference terms at $T=66.9$ MeV and electron-scattering angle of 60°. The bremsstrahlung and interference terms are negligible apart from photon directions near the incident and scattered electron directions or diffraction minima. Note that, for ^{12}C, Coulomb distortion plays a significant role with a small shift in the photon angular distribution, but with a significant change in the magnitude of the total cross section. In Fig. 1(b) we show the Coulomb distortion effects on the total coincidence cross section at electron incident energy $E_i=66.9$ MeV and scattering angle of $\theta_e=60°$. As noted earlier, the DWBA calculation for bremsstrahlung does not converge for photon angles too near the electron incident and final direction, and so we only show the DWBA results in angular regions where we achieve convergence. In Fig. 1(c) we show our DWBA calculation as compared to the experimental data from Illinois [12]. The experimental data were not an absolute measurement and have been shifted to obtain a best fit which is excellent. Our results are in general agreement with those of Ravenhall *et al.* [11], in that we confirm their conclusion regarding the sign between the longitudinal and transverse form factors, but our agreement with the data is somewhat better. We suspect this arises from their approximate treatment of the Coulomb effects on the transverse terms. Note that the full PWBA and DWBA curves are very slightly shifted in angle for this case; the primary effect is a change in magnitude.

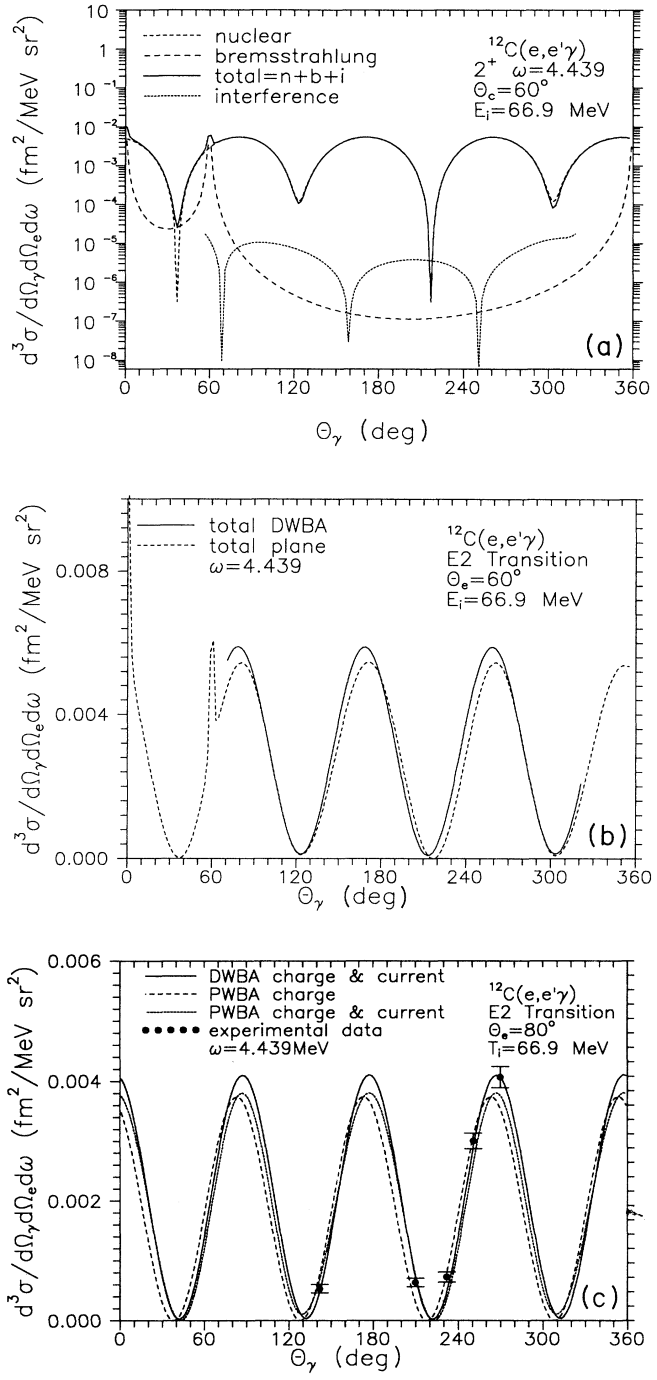

FIG. 1. (a) Coincidence cross sections for $^{12}C(e,e'\gamma)$ as a function of photon polar angle θ_γ. The curves labeled nuclear and bremsstrahlung are the cross section for these two processes, the curve labeled interference is the absolute magnitude of the interference term between nuclear and bremsstrahlung, and the curve labeled total is the coherent sum of both processes. (b) Coulomb distortion effects on the total coincidence cross section for $^{12}C(e,e'\gamma)$ as a function of photon polar angle θ_γ. Note that the DWBA calculation for bremsstrahlung does not converge for photon angles too near the electron incident and final direction. (c) Same as (b) except the electron scattering angle is 80°. The experimental data is from Ref. [12].

B. ^{90}Zr$(e,e'\gamma)(7^+, 5.06$ MeV)

To investigate Coulomb distortion and bremsstrahlung contributions in a medium nuclei, we consider the case of an $M7$ transition from the spin-0 ground state to the 5.060-MeV 7^+ state in ^{90}Zr which has been studied using inelastic electron scattering by Heisenberg *et al.* [18]. They performed a *model-independent* reconstruction of the current density $J_{L,L}(r)$ for the pure magnetic transition using the Fourier-Bessel expansion, and we have used their results. In Fig. 2(a) we show the coincidence differential cross sections for nuclear excitation and deexcitation, bremsstrahlung, and the interference terms for $T=100$ MeV. In this case bremsstrahlung alone is not very significant, but there is a significant interference effect. In Fig. 2(b) we show the Coulomb distortion effects on the total coincidence cross section at electron incident energy $T=100$ MeV and scattering angle of $\theta_e=60°$. Recall that we can only show DWBA results in the angular region where we achieve convergence. In order to check the energy dependence of Coulomb distortion, we varied the incident energy of electron and as expected, the Coulomb distortion reduces significantly with an increase of the incident electron energy from 100 to 150 MeV as shown in Figs. 2(c) and 2(d).

C. ^{208}Pb$(e,e'\gamma)(3^-, 2.615$ MeV)

To investigate Coulomb distortion and the bremsstrahlung contribution in a heavy nuclei, we examine the excitation of the first the 3^- state in ^{208}Pb and subsequent gamma decay back to the ground state. We use the transition charge and current distributions from the Tassie model [1] for ^{208}Pb as normalized by the inelastic data given by Heisenberg *et al.* [18]. In Fig. 3(a) we show the coincidence differential cross section for nuclear excitation deexcitation, bremsstrahlung, and the interference terms at $T=100$ MeV and scattering angle of $\theta_e=60°$. In this case the interference term contributes 5–10 % away from the bremsstrahlung peaks. This is a very collective transition [the $B(E3)$ is approximately 29 single-particle units], and so the nuclear excitation and deexcitation dominates. In Fig. 3(b) we show the distortion effect on the bremsstrahlung coincidence cross section at $T=100$ MeV and scattering angle of electron $\theta_e=60°$. The distortion effects on the bremsstrahlung cross section are comparable to those on the nuclear excitation and deexcitation cross section. As usual, we only show DWBA results in the angular region where we achieve convergence in the bremsstrahlung cross section. To examine the prospects of looking at a single-particle transition in such a heavy nucleus, we repeated the above calculation with the $B(E3)$ value reduced by a factor of 29 and show the results in Fig. 3(c). Note that while both bremsstrahlung and the interference terms contribute significantly, the distinctive octupole pattern remains.

D. ^{181}Ta$(e,e'\gamma)(\frac{9}{2}^+, 0.136$ MeV)

We again used the Tassie model for the $\frac{7}{2}-\frac{9}{2}^+$ (0.136 MeV) excitation in ^{181}Ta for the charge and current dis-

tributions. This transition can be mediated via $M1, E2, M3, E4, \ldots, E8$, but since the photon energy ω is so small, it is dominated by the $M1$ and $E2$ transitions. The reduced transition probabilities $B(E2)=19\,000$ $e^2\,\mathrm{fm}^4$ and $B(M1)=1.28\times10^{-3}\ e^2\,\mathrm{fm}^2$, as determined by Armbruster *et al.* [19], were used for absolute normalization. In Fig. 4(a) we show the coincidence cross section for nuclear excitation and deexcitation, bremsstrahlung, and the interference terms at $T=30$ MeV. In this case neither bremsstrahlung nor the interference terms are significant. While the strength of the $E2$ and $M1$ transitions has been determined, the relative phase of the transition amplitude is not known. In order to investigate the dependence of the photon angular distribution on the relative sign between electric and magnetic transition matrix elements, we show the effects of choosing a positive and negative relative sign in Fig. 4(b). We find a significant change in the angular distribution pattern, and from this information we could easily extract the relative sign if we were to have experimental results. In Fig. 4(c) we also show what patterns would be produced for a pure electric ($E2$) or pure magnetic ($M1$) transition.

E. ^{15}N$(e,e'\gamma)(\frac{3}{2}^-, 6.32\ \mathrm{MeV})$

The next case we consider is the excitation of the spin $-\frac{1}{2}^-$ grand state of ^{15}N to the $\frac{3}{2}^-$ state at 6.32 MeV and deexcitation by photon emission back to the ground state. We use the Fourier-Bessel fit to the transition charge distribution of Nick [13] and analytic forms for the transverse electric and magnetic form factors given by Donnelly, Raskin, and Dubach [9] to characterize this mixed transition. For an $E2$-$M1$ mixed transition, there will generally be a single Coulomb multipole, but two transverse multipoles (one electric and one magnetic). Measurements of the angular distribution for a well-chosen set of electron and photon angles may then be used to determine not only the transverse-longitudinal interference, but also the transverse-transverse nuclear interference and, thereby, to separate the two transverse multipoles ($E2$ and $M1$). The reduced transition probability $B(E2)=14.4\ e^2\,\mathrm{fm}^4$ and $B(M1)=1.43\times10^2\ e^2\,\mathrm{fm}^2$ for the decay have been determined by Shukla and Brown [20]. In Fig. 5(a) we show the nuclear excitation and deexcitation, bremsstrahlung, and interference contribu-

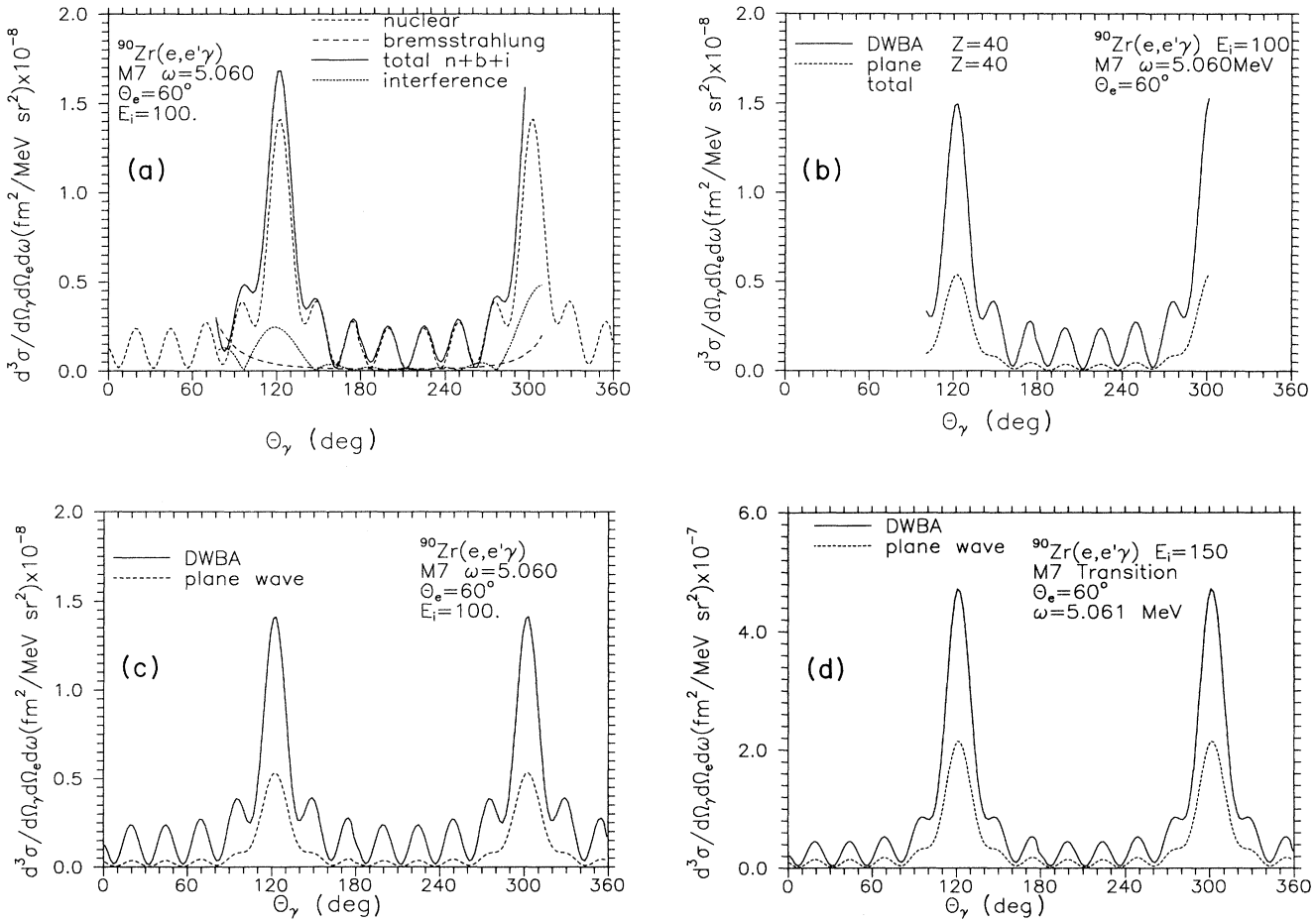

FIG. 2. (a) Same as in Fig. 1(a) for ^{90}Zr$(e,e'\gamma)$. (b) Same as in Fig. 1(b) for ^{90}Zr$(e,e'\gamma)$. (c),(d) DWBA and plane-wave coincidence cross sections for ^{90}Zr$(e,e'\gamma)$ as a function of photon polar angle θ_γ for the electron incident energies $T=100$ and 150 MeV, respectively.

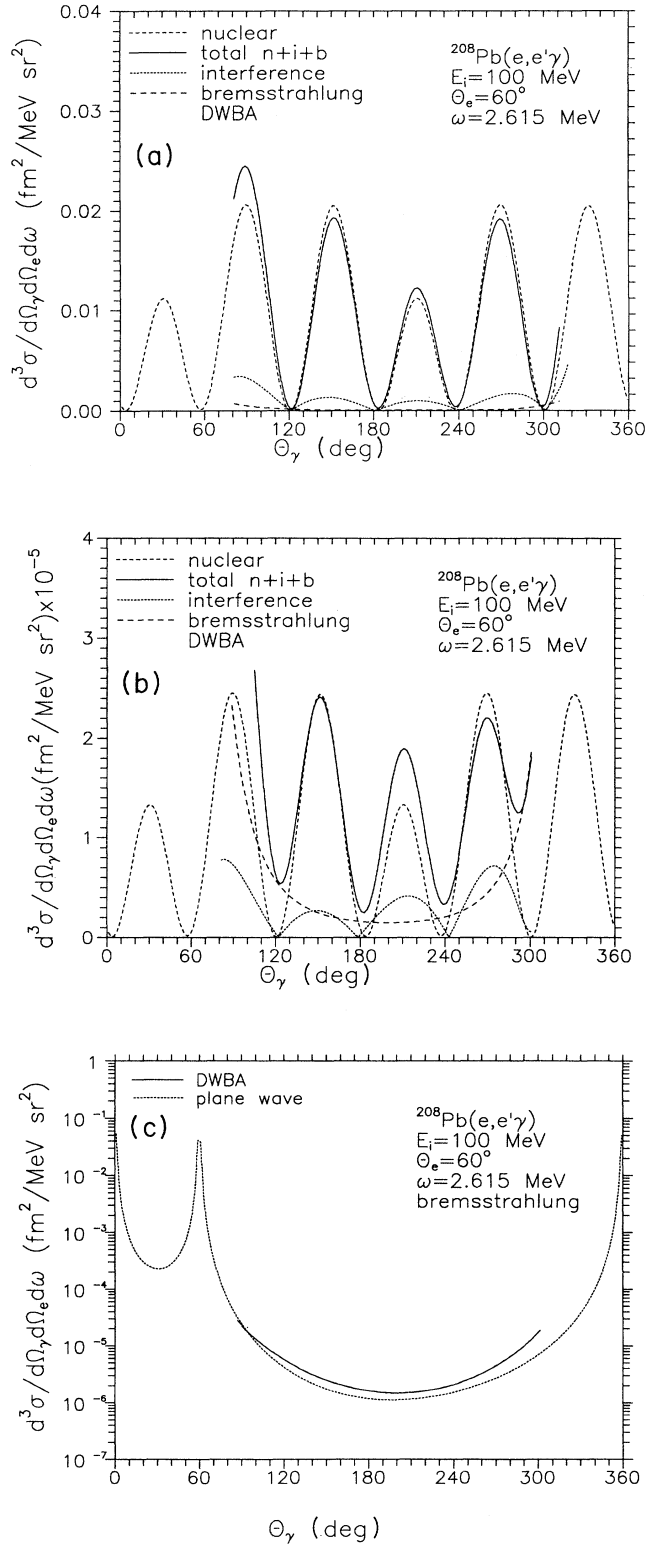

FIG. 3. (a) Same as in Fig. 1(a) for ^{208}Pb$(e,e'\gamma)$. (b) Same as in (a) for ^{208}Pb$(e,e'\gamma)$ except that a single-particle value was used for $B(E3)$. (c) Coincidence cross sections due to bremsstrahlung for ^{208}Pb$(e,e'\gamma)$ as a function of photon polar angle θ_γ.

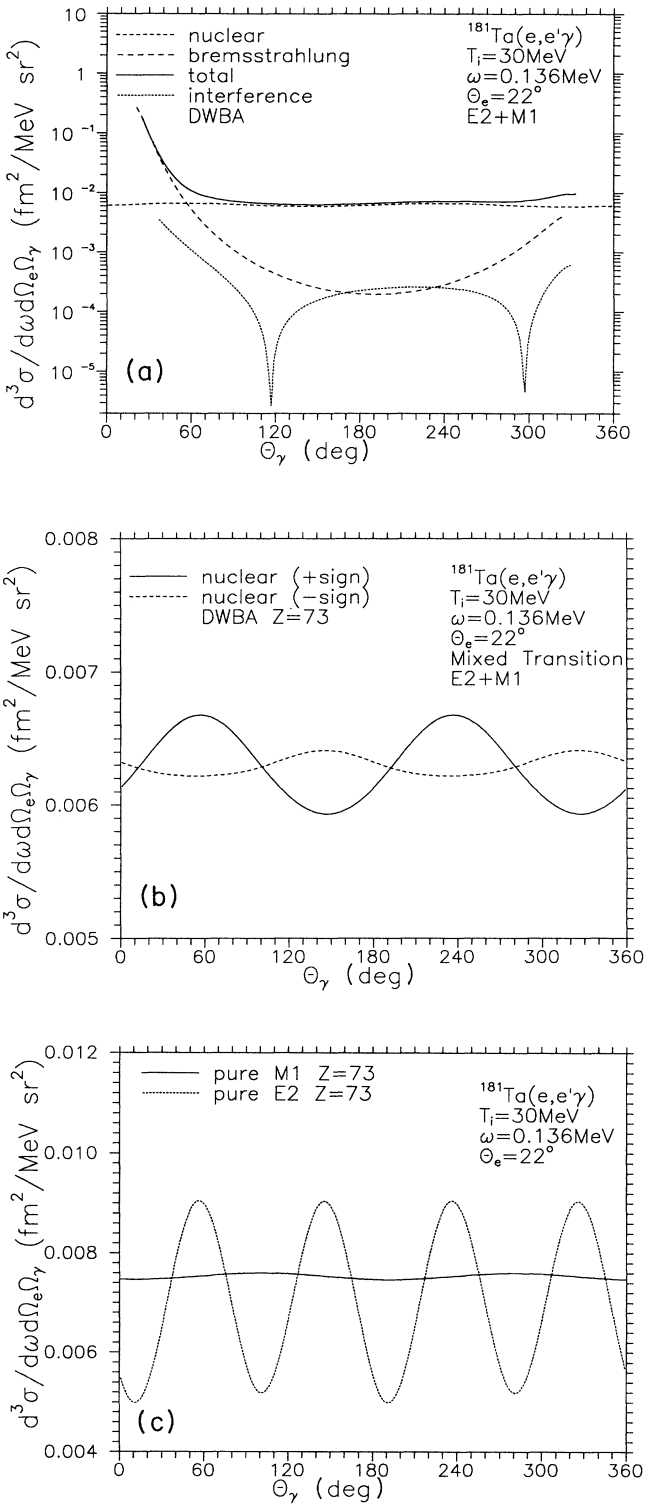

FIG. 4. (a) Same as in Fig. 1(a) for ^{181}Ta$(e,e'\gamma)$. (b) Coincidence nuclear excitation and deexcitation cross sections for ^{181}Ta$(e,e'\gamma)$ with relative sign change between electric and magnetic matrix elements, as function of photon polar angle θ_γ. (c) Coincidence nuclear excitation and deexcitation coincidence cross sections for pure electric ($E2$) and magnetic ($M1$) transitions, as function of photon polar angle θ_γ.

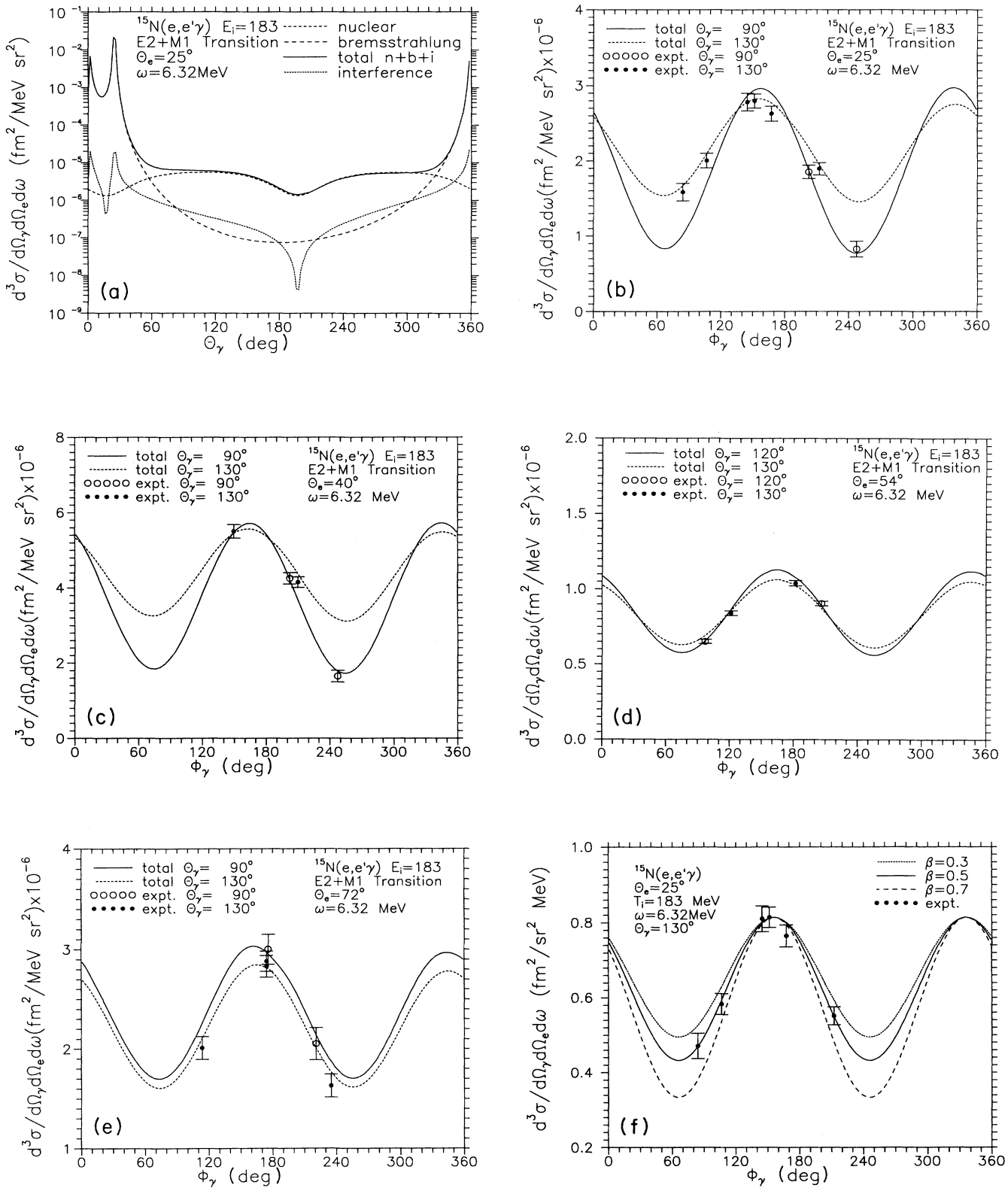

FIG. 5. (a) Same as in Fig. 1(a) for ^{15}N$(e,e'\gamma)$. (b)–(e) Coincidence cross section for ^{15}N$(e,e'\gamma)$ as function of photon azimuthal angle ϕ_γ, calculated in plane wave. (f) Same as in (b)–(e) except that the very small interference and bremsstrahlung terms are neglected. In order to check sensitivity of the $E2$ and $M1$ strength, we varied the mixing parameter β. (g) Coincidence cross sections for ^{15}N$(e,e'\gamma)$ as a function of photon polar angle θ_γ. Here we varied the mixing parameter β at $T=96.3$ MeV.

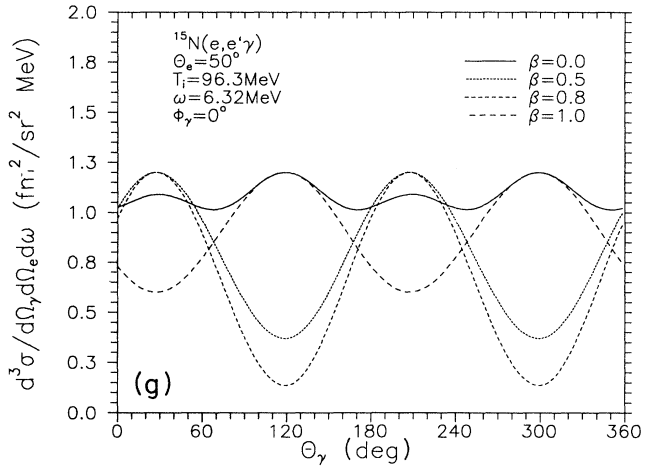

FIG. 5. (*Continued*).

tions to the differential cross section at $T=183$ MeV and scattering angle of electron $\theta_e=25°$. In this case bremsstrahlung and the interference terms are only significant near the incident and scattered electron angles. In Figs. 5(b)–5(e) we show a comparison of our calculations with the experimental results carried out at the University of Mainz by Nick [13]. The photon angular distributions were measured for various polar angles as a function of the out-of-plane azimuthal angle ϕ_γ. Recalling that we have defined the electron azimuthal angle as 0, we set the electron-scattering angles $\theta_e=24°$, 40°, 54°, and 72° and fixed the photon polar angle θ_γ at 90°, 120°, and 130° while varying ϕ_γ. In general, our calculated shapes are in very good agreement with the measured distributions. Note that only relative cross sections were measured, and so we multiplied the data points of a given azimuthal distribution by a factor which gives the best fit to our calculated cross sections. While Coulomb distortion effects result in small shifts in the θ_γ distribution we only found an overall magnitude change in a given ϕ_γ distribution. Hence this experiment is not sensitive to Coulomb effects. In order to check the sensitivity of the nuclear excitation and deexcitation to the relative strength of the $E2$ and $M1$, we varied the β factor in Eq. (35) to obtain the azimuthal distributions shown in Fig. 5(f) for $T=183$ MeV, electron-scattering angle $\theta_e=25°$, and photon polar angle $\theta_\gamma=130°$. The experimentally determined $B(E2)$ and $B(M1)$ corresponds to $\beta=0.5$ and gives the best fit to the data. Increasing or decreasing β results in quite different shapes. In Fig. 5(g) we varied the β factor for photon polar angle distributions for $T=96.3$ MeV, scattering electron angle $\theta_e=50°$, and photon azimuthal angle $\phi_\gamma=0°$. Again, we find that the shapes for different admixtures are quite different, and so it should be possible to extract the mixing parameter.

IV. SUMMARY AND CONCLUSION

We have a working calculation for the $(e,e'\gamma)$ process which treats the Coulomb distortion of electrons exactly using solutions of the Dirac equation with the static Coulomb potential of the nucleus included. The ingredients needed for studying a given nuclear excitation and deexcitation process are multipole decomposed transition charge and current radial distributions. In the preceding section we investigated the $(e,e'\gamma)$ process for a number of different nuclear excitations and subsequent deexcitations described by various simple models which have been fitted to inelastic electron-scattering data. We have carried out our calculations using the plane-wave approximation and the distorted-wave Born approximation, and in both calculations we have included the accompanying bremsstrahlung amplitude which contributes coherently for nuclear deexcitations back to the ground state. We have concentrated our attention on examining the gamma angular distributions both in and out of the scattering plane defined by incident and scattered electron directions.

The Coulomb distortion effects are not very large for light nuclei, but they do result in small shifts in the angular distributions and should be included when one is sorting out transverse and longitudinal parts of the excitation process. We also note that Coulomb distortion leads to changes in the absolute value of the cross section which would be important for absolute normalization measurements. For medium and heavy nuclei, the Coulomb distortion effects are quite large in both the nuclear excitation process and accompanying bremsstrahlung process, but in the cases we examined, they do not cause any difficulty in examining the photon angular distributions. That is, sensitivity to mixed multipoles is still present, and this reaction can be a very useful tool for determining the various multipole components and their relative phases in mixed transition.

We have also included the bremsstrahlung contributions in both the plane-wave and DWBA calculations. If we avoid detection of photons within 30°–40° of either the incident or scattered electron direction, the bremsstrahlung contributions for the light nuclei can usually be ignored, although the interference term makes small contributions. For medium and heavy nuclei, the bremsstrahlung contributions increase, but even for single-

particle transitions the nuclear excitation and deexcitation gamma distinctive multipole patterns can still be clearly seen. This is because the bremsstrahlung photon distributions tend to be rather smooth with respect to angle apart from the peaks around the incident and outgoing electron directions.

We have demonstrated with a number of examples that the $(e,e'\gamma)$ appear to very useful in analyzing mixed-multipole transitions in nuclei. While Coulomb distortion effects and the bremsstrahlung contributions need to be included, particularly for heavy nuclei, they do not significantly reduce the utility of this reaction in doing nuclear spectroscopy.

ACKNOWLEDGMENTS

We thank Yanhe Jin for a number of useful suggestions and the Ohio Supercomputer center for time on the Cray Y-MP. This research was supported in part by the grant from the Geneseo Research Foundation and in part by the U.S. Department of Energy under Grant No. FG02-87ER40370.

APPENDIX: CHARGE AND CURRENT DENSITIES

In PWBA the form factors F_L are simple Fourier-Bessel transforms of the nuclear charge and current densities and are given in terms of the transition charge and current densities $\rho_L(r)$ and $J_{L,L'}(r)$ as

$$F_L^c(q)=\int_0^\infty \rho_L(r) j_L(qr) r^2 dr \ , \tag{A1}$$

$$F_L^E(q)=\frac{1}{\hat{L}}\int_0^\infty [\sqrt{L+1}\,J_{L,L-1}(r) j_{L-1}(qr) - \sqrt{L}\,J_{L,L+1}(r) j_{L+1}(qr)] r^2 dr \ , \tag{A2}$$

$$F_L^M(q)=\int_0^\infty J_{L,L}(r) j_L(qr) r^2 dr \ , \tag{A3}$$

where C, E, and M represent Coulomb, transverse electric, and transverse magnetic, respectively. The continuity equation, which is just a statement of charge conservation, connects the currents $J_{L,L+1}$ and $J_{L,L-1}$ to the transition charge ρ_L by

$$\hat{L}\omega\rho_L(r)=\sqrt{L}\left[\frac{d}{dr}-\frac{L-1}{r}\right]J_{L,L-1}(r) - \sqrt{L+1}\left[\frac{d}{dr}+\frac{L+2}{r}\right]J_{L,L+1}(r) \ , \tag{A4}$$

where $\hat{L}=\sqrt{2L+1}$. After Fourier transformation the continuity equation becomes

$$\frac{\omega\hat{L}}{q}F_L^c(q)=-\sqrt{L}\,F_{L,L-1}(q)-\sqrt{L+1}\,F_{L,L+1}(q) \ , \tag{A5}$$

which can be used to eliminate $J_{L,L-1}(r)$ so that the transverse electric form factor becomes

$$F_L^E(q)=-\left[\frac{L+1}{L}\right]^{1/2}\frac{\omega}{q}F_L^c(q) - \frac{\hat{L}}{\sqrt{L}}\int J_{L,L+1}(r) j_{L+1}(qr) r^2 dr \ . \tag{A6}$$

Finally, since the measured form factors are just Fourier-Bessel transforms of the densities, they can be inverted to obtain

$$\rho_L(r)=\frac{2}{\pi}\int_0^\infty F_L^c(q) j_L(qr) q^2 dq \ ,$$

$$J_{L,L+1}(r)=-\frac{2}{\pi}\frac{\sqrt{L}}{\hat{L}}\int_0^\infty \left[F_L^E(q) + \left[\frac{L+1}{L}\right]^{1/2}\frac{\omega}{q}F_L^c(q)\right] \times j_{L+1}(qr) q^2 dq \ ,$$

$$J_{L,L}(r)=\frac{2}{\pi}\int_0^\infty F_L^M(q) j_L(qr) q^2 dq \ .$$

[1] S. T. Tuan, L. E. Wright, and D. S. Onley, Nucl. Instrum. Methods **60**, 70 (1968).
[2] Indu Talwar, L. E. Wright, D. S. Onley, and Soto Vargas, Phys. Rev. C **35**, 510 (1987).
[3] Indu Talwar, L. E. Wright, and A. Hoque, Phys. Rev. C **41**, 382 (1990).
[4] D. F. Hubbard and M. E. Rose, Phys. Rev. **181**, 337 (1966).
[5] H. L. Acker and M. E. Rose, Ann. Phys. **44** (N.Y.) 366 (1967).
[6] D. Drechsel and H. Überall, Phys. Rev. **181**, 1383 (1969).
[7] H. Arenhövel and D. Drechsel, Nucl. Phys. **A233**, 153 (1974).
[8] E. Fein, D. Drechsel, M. Cavinato, M. Marangoni, and A. M. Saruis, Nucl. Phys. **A468**, 301 (1987).
[9] T. W. Donnelly, A. S. Raskin, and J. Dubach, Nucl. Phys. **A474**, 307 (1987).
[10] T. A. Griffy and D. Whitehill, Phys. Rev. C **2**, 441 (1970).
[11] D. G. Ravenhall, R. L. Schult, J. Wambach, C. N. Papanicolas, and S. E. Williamson, Ann. Phys. (N.Y.) **178**, 187 (1987).
[12] C. N. Papanicolas, S. E. Williamson, H. Rothhaas, G. O. Bolme, L. J. Koester, Jr., B. Miller, R. Miskimen, P. Mueller, and L. S. Cardman, Phys. Rev. Lett. **54**, 26 (1985).
[13] Rainer Nick, diploma, University of Mainz, 1988.
[14] C. N. Papanicolas, invited talk presented at the *Third International Workshop on Perspective on Nuclear Physics* (International Center for Theoretical Physics, Trieste, Italy, 1987).
[15] M. E. Rose, *Elementary Theory of Angular Momentum* (Wiley, New York, 1957).
[16] D. R. Yennie and D. G. Ravenhall, Phys. Rev. **95**, 500 (1954).

[17] J. M. Eisenberg and W. Greiner, *Excitation Mechanism of the Nucleus* (North-Holland, Amsterdam, 1970), Vol. II.
[18] J. Heisenberg, J. Dawson, T. Millman, O. Schwentker, J. Lichternstadt, C. N. Papanicolas, J. Wise, J. S. McCarthy, N. Hintz, and H. P. Blok, Phys. Rev. C **29**, 97 (1984).
[19] R. Armbruster, Y. Gerber, A. Macher, and J. P. Vivien Nucl. Phys. **A143**, 315 (1970).
[20] A. P. Shukla, G. E. Brown, Nucl. Phys. **A112**, 296 (1968).